HSC-XD 52: An X-Ray Detected AGN in a Low-mass Galaxy at $z \sim 0.56$

Goni Halevi[1] , Andy Goulding[1], Jenny Greene[1], Jean Coupon[2], Anneya Golob[3], Stephen Gwyn[4], Sean D. Johnson[1,5,10] ,
Thibaud Moutard[3], Marcin Sawicki[3,4,11], Hyewon Suh[6,12] , and Yoshiki Toba[7,8,9]

[1] Department of Astrophysical Sciences, Princeton University, 4 Ivy Lane, Princeton, NJ 08544, USA; ghalevi@princeton.edu
[2] Department of Astronomy, University of Geneva, ch. d'Ecogia 16, 1290, Versoix, Switzerland
[3] Department of Astronomy & Physics, Institute for Computational Astrophysics, Saint Mary's University, Halifax, Canada
[4] NRC Herzberg Astronomy and Astrophysics, 5071 West Saanich Road, Victoria, BC V9E 2E7, Canada
[5] The Observatories of the Carnegie Institution for Science, 813 Santa Barbara Street, Pasadena, CA 91101, USA
[6] Subaru Telescope, National Astronomical Observatory of Japan, 650 North A'ohoku Place, Hilo, HI 96720, USA
[7] Department of Astronomy, Kyoto University, Kitashirakawa-Oiwake-cho, Sakyo-ku, Kyoto 606-8502, Japan
[8] Academia Sinica Institute of Astronomy and Astrophysics, 11F of Astronomy-Mathematics Building, AS/NTU, No.1, Section 4, Roosevelt Road, Taipei 10617, Taiwan
[9] Research Center for Space and Cosmic Evolution, Ehime University, 2-5 Bunkyo-cho, Matsuyama, Ehime 790-8577, Japan
Received 2019 June 28; revised 2019 September 27; accepted 2019 October 4; published 2019 October 23

Abstract

The properties of low-mass galaxies hosting central black holes provide clues about the formation and evolution of the progenitors of supermassive black holes. In this Letter, we present HSC-XD 52, a spectroscopically confirmed low-mass active galactic nucleus (AGN) at an intermediate redshift of $z \sim 0.56$. We detect this object as a very luminous X-ray source coincident with a galaxy observed by the Hyper Suprime-Cam (HSC) as part of a broader search for low-mass AGN. We constrain its stellar mass through spectral energy distribution modeling to be LMC-like at $M_\star \approx 3 \times 10^9 M_\odot$, placing it in the dwarf regime. We estimate a central black hole mass of $M_{\rm BH} \sim 10^6 M_\odot$. With an average X-ray luminosity of $L_{\rm X} \approx 3.5 \times 10^{43}$ erg s^{-1}, HSC-XD 52 is among the most luminous X-ray selected AGN in dwarf galaxies. The spectroscopic and photometric properties of HSC-XD 52 indicate that it is an intermediate-redshift counterpart to local low-mass AGN.

Unified Astronomy Thesaurus concepts: Supermassive black holes (1663); Dwarf galaxies (416); X-ray active galactic nuclei (2035)

1. Introduction

Supermassive black holes (SMBHs) are thought to play a crucial role in galaxy evolution. SMBHs are ubiquitous in present-day massive galaxies and their properties correlate with those of their hosts (for a review, see Kormendy & Ho 2013). Observations of central black holes in dwarf galaxies over cosmic time may provide insight into the birth and growth of SMBHs. Simulations predict that these low-mass black holes experience relatively little growth via mergers or accretion (Bellovary et al. 2011), allowing them to serve as indirect probes of the black holes that seed the SMBHs observed in massive galaxies today.

At present, we know little about the demographics of central black holes in low-mass galaxies, even in the local universe. The dynamical signatures of $\sim 10^5 M_\odot$ massive black holes (MBH) are found in some, but not all, galaxies within 3.5 Mpc with $M_\star \approx 10^9$–$10^{10} M_\odot$ (Nguyen et al. 2019). The dearth of information about black holes in this regime not only limits our understanding of SMBH seeds but also impedes predictions of gravitational-wave events detectable by LISA and their rates (e.g., Bellovary et al. 2019).

Statistical constraints on the black hole occupation fraction require a large survey of black holes in low-mass ($M_\star \lesssim 10^{10} M_\odot$) hosts. Searches with optical emission lines (e.g., Ho et al. 1997; Greene & Ho 2007; Dong et al. 2012; Reines et al. 2013; Moran et al. 2014), mid-infrared (IR) spectroscopy (e.g., Satyapal et al. 2009), and radio continuum

(e.g., Reines et al. 2014) have all yielded interesting samples. We focus on X-ray searches, which provide an unbiased measure of the accretion luminosity, and are relatively insensitive to obscuration (e.g., Brandt & Alexander 2015).

X-ray observations are a powerful tool to study MBH demographics locally (e.g., Desroches & Ho 2009; Gliozzi et al. 2009; McAlpine et al. 2011; Araya Salvo et al. 2012; Secrest et al. 2012; Lemons et al. 2015; She et al. 2017); they place the only accretion-based constraint on the occupation fraction ($> 20\%$; Miller et al. 2015). Pushing to higher redshift is enabled by ongoing deep X-ray observations (e.g., Schramm et al. 2013; Bizzocchi et al. 2014), but it is very challenging to understand the completeness of spectroscopic samples (Pardo et al. 2016) and the purity of photometric samples (Mezcua et al. 2018).

In this Letter, we present one tantalizing object from our new search for such sources, which uses the relatively wide survey area and sensitivity of the Deep Layer of the Hyper Suprime-Cam Subaru Strategic Program (HSC-D; Aihara et al. 2018b) and the complementary CFHT Large Area U-band Deep Survey (CLAUDS; Sawicki et al. 2019) to find faint low-mass galaxies (G. Halevi et al. 2019, in preparation). We conducted our search in the *XMM-Newton* Large-Scale Structure (XMM-LSS) field, where we used the SEXTRACTOR-based u^*grizy catalog produced by the CLAUDS team (A. Golob et al. 2019, in preparation; see also Section 3.1.2 in Sawicki et al. 2019). This catalog extends the HSC photometric sampling, enabling improved estimates of the redshift, stellar mass ($M_\star$), and star formation rate (SFR) for each source (T. Moutard et al. 2019, in preparation). To identify candidates for our sample of HSC X-ray Dwarfs (HSC-XDs), we cross-matched candidate dwarf

---

Table 1
Properties of HSC-XD 52

α	δ	XMM ID	z
02:24:15.76	$-05:27:20.02$	XMM03471	0.561
i (mag)	$g - r$ (mag)	$f_{0.5-2\,keV}$ (erg cm^{-2} s^{-1})	$f_{0.5-10\,keV}$ (erg cm^{-2} s^{-1})
21.479 $\pm$0.008	0.542 $\pm$0.011	(4.5 ± 0.6) $\times 10^{-15}$	(2.8 ± 0.2) $\times 10^{-14}$
$M_\star$ ($10^9\,M_\odot$)	SFR ($M_\odot$ yr^{-1})	Ψ	L_{AGN} (10^{43} erg s^{-1})
3.0 ± 0.7	5.76 ± 0.56	$40°$	9.56 ± 0.48
$\log\left(\frac{[OI]}{H\alpha}\right)$	$\log\left(\frac{[O\,ddIII]}{H\beta}\right)$	$f_{H\alpha}$ (erg cm^{-2} s^{-1})	$f_{[O\,III]}$ (erg cm^{-2} s^{-1})
-0.75	1.04	1.1×10^{-15}	5.4×10^{-16}

galaxies in this catalog with the XMM-SERVS source catalog (Chen et al. 2018).

The source presented in this Letter, hereafter referred to as HSC-XD 52, is an intermediate-redshift low-mass AGN observed at multiple epochs in both X-ray imaging and optical spectroscopy. The galaxy has a dwarf-like stellar mass and hosts a luminous X-ray detected AGN that is seen to be declining in activity with time. Its position, basic properties, and derived best-fit parameters are provided in Table 1.

2. A Luminous X-Ray Source in a Dwarf Galaxy

HSC-XD 52 is of particular interest because the available data not only confirms its (time-evolving) AGN nature but also strongly implies a low stellar mass ($<10^{10}M_\odot$; assuming a Chabrier initial mass function). The HSC imaging shows a marginally extended red galaxy (top left panel of Figure 1; Table 1). The XMM-SERVS data reveal a luminous X-ray source (top right panel of Figure 1) spatially coincident with the optically detected galaxy. Its X-ray properties are described in Section 4. The three epochs of XMM observations spanning 2006–2017 show temporal variability indicative of a fall in X-ray luminosity.

The Sloan Digital Sky Survey (SDSS; Blanton et al. 2017) obtained a spectrum of HSC-XD 52 despite its relative optical faintness ($i = 21.5$ mag) because it was targeted as part of the XMM-XXL follow-up program. We additionally acquired a spectrum on 2019 July 27 with the *Magellan* Echellette (MagE) Spectrograph, a moderate-resolution ($R \sim 4100$ for a 1″ slit) optical echellette mounted on the Clay *Magellan* II telescope. While the SDSS spectrum from 2013 suggests the presence of broad lines indicative of accretion onto an MBH, this evidence is not present in the 2019 spectrum despite its higher resolution and signal-to-noise ratio (S/N). The broadband spectral energy distribution (SED) presented in Figure 2 and discussed in Section 3 supports the classification of this source as an AGN in a dwarf galaxy, as do its early-epoch X-ray properties and the ratios of its narrow emission lines. The combination of these properties points toward the characterization of HSC-XD 52 as a higher-redshift analog of the $z \sim 0$ low-mass AGN POX 52 (Barth et al. 2004) and NGC 4395 (Filippenko & Ho 2003), though one with a accretion rate that is decreasing with time.
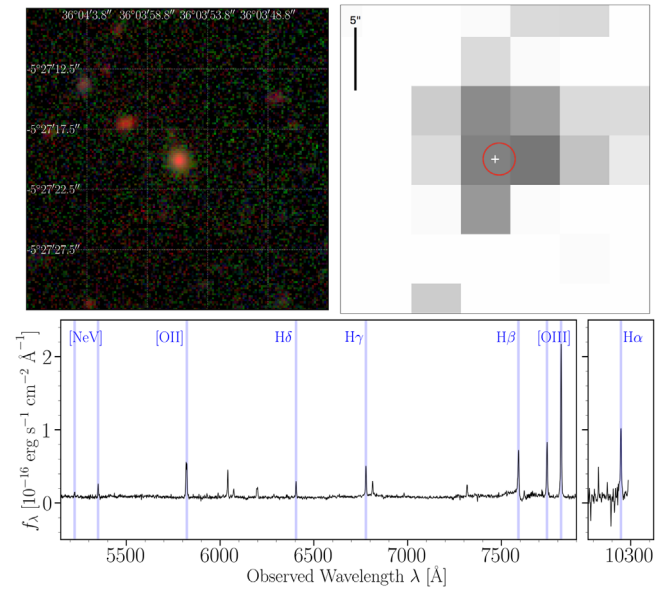

Figure 1. HSC-D *gri* composite image (top left), XMM full-band image (top right), and smoothed MagE spectrum (bottom) of HSC-XD 52. The images span 25″ on each side. The overlaid grid has spacings of 5″. The XMM image uses an inverted logarithmic color scale. The white cross marks the XMM centroid, whereas the red circle with a radius of 1″3 is centered on the HSC position. We note that the Hβ emission line is blended with a strong sky line; its apparent broadness and asymmetry are not intrinsic.

3. Constraining the Stellar Mass

Our initial estimate of the stellar mass, $M_\star \approx 4 \times 10^9 M_\odot$, was derived from photometric template-fitting of the HSC *grizy*, CLAUDS $u^\star$, and *Galaxy Evolution Explorer* (*GALEX*) data (see T. Moutard et al. 2019, in preparation), following the procedure described by Moutard et al. (2016). We utilized additional photometry from *Spitzer* IRAC and MIPS, *Herschel* SPIRE (Griffin et al. 2010), and the VISTA Deep Extragalactic Observations survey (see Aihara et al. 2018a and references therein) to further constrain $M_\star$ using a multiwavelength SED fit with the Code Investigating GALaxy Emission (CIGALE[13]; Noll et al. 2009; Boquien et al. 2019). In calculating the SED model, we used the stellar population models of Bruzual & Charlot (2003), the Chabrier (2003) initial mass function, an exponentially declining delayed star formation history, a dusty star-forming template from Dale et al. (2014), and the AGN torus models of Fritz et al. (2006) allowing for a range of optical depths and inclinations. We fixed the extinction using the Balmer decrement from the Hα/Hβ ratio ($A_V = 1.3$; see Section 4), though we recover a similar A_V when leaving it as a free parameter. The observed SED and CIGALE models are shown in Figure 2. The best-fit model, for which we also show the residuals (middle panel), has $\chi^2_{n-1} = 2.87$ indicating a formally poor fit. However, this is expected because we exclude nebular/AGN emission lines in the templates. The photometric points that contribute most to raising the χ^2 value are the HSC-i and HSC-Y bands, which fall precisely at the wavelengths including the high-equivalent width [O III] and Hα lines. These are underestimated by our SED model.

The best-fit stellar model has $M_\star \approx (3.0 \pm 0.7) \times 10^9 M_\odot$, consistent with our initial estimate from CLAUDS, stellar population age ~ 0.5 Gyr, and SFR $\approx (5.76 \pm 0.56)$ $M_\odot$ yr^{-1}.
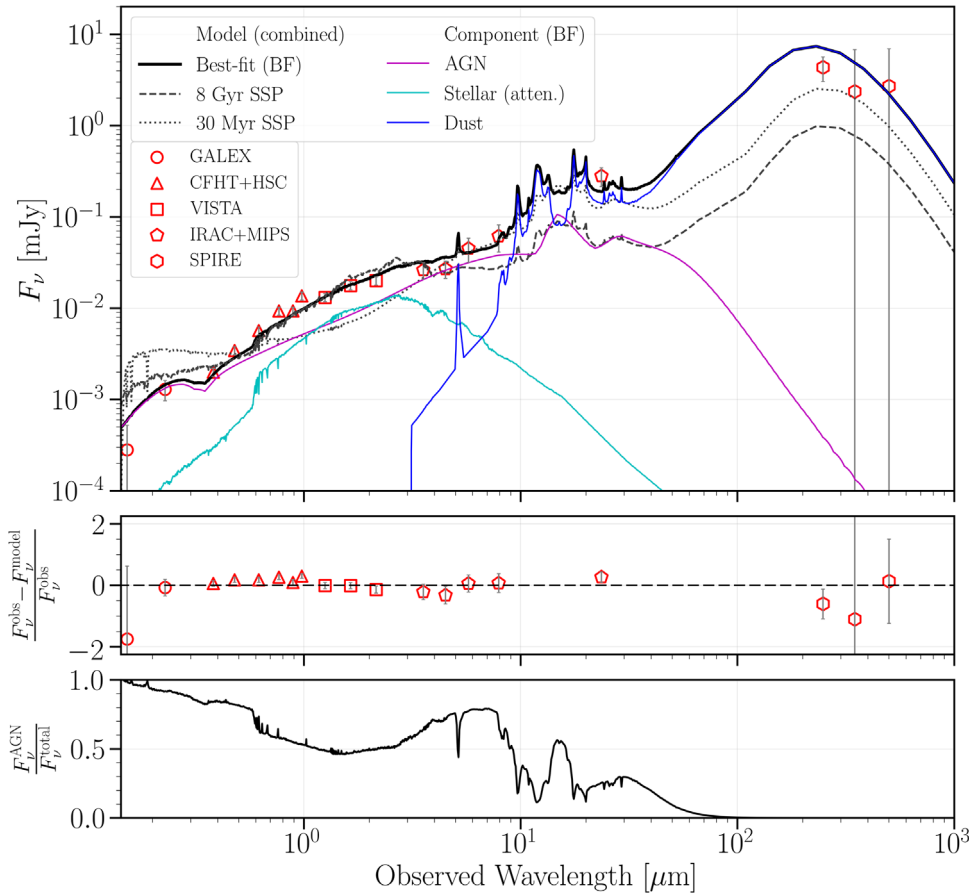
Figure 2. Result of SED modeling using CIGALE. Top panel: the best-fit model (solid black line) and two models with fixed single stellar populations (SSPs; gray lines) of ages 8 Gyr (dashed) and 30 Myr (dotted). Red symbols show photometric observations (which represent total magnitudes because the galaxy is barely resolved even in HSC) and relative residuals (middle panel) with shapes indicating different instruments or surveys. Error bars represent 1σ statistical uncertainties with a 1% systematic floor. Bottom panel: ratio of AGN to total emission in the best-fit model.

The AGN component dominates the rest-frame optical emission (see the bottom panel of Figure 2), favoring an intermediate inclination of $\Psi \approx 40°$, placing HSC-XD 52 closer to the Type 1 regime (i.e., mostly unobscured).

To obtain a conservative $M_\star$ upper limit, we ran CIGALE with the same input ranges but required a fixed single stellar population (SSP) of 8 Gyr (the age of the universe at $z \approx 0.5$). The upper limit of $M_\star < 1.1 \times 10^{10} M_\odot$ is shown as a gray dashed line in Figure 2. Furthermore, we found a fixed SSP of 30 Myr (i.e., a very young stellar population; dotted gray line in Figure 2) fails to reproduce the observed photometry.

Our case for the low stellar mass of the host galaxy is strengthened by spectral indicators of its low metallicity. In particular, both the SDSS spectrum and the higher-resolution, higher-S/N MagE spectrum show a complete lack of evidence for [N II] $\lambda6548, \lambda6583$ lines (see the top panels of Figure 4). We can put a limit on the line strength compared to Hα from the MagE spectrum of [N II]/H$\alpha \lesssim -1.8$. From the models of Groves et al. (2006), we then place the metallicity at $\lesssim 0.25 Z_\odot$, where $Z_\odot$ represents solar metallicity. Given the well-known stellar mass–metallicity relation, we can conclude by this entirely complementary line of evidence that HSC-XD 52 indeed qualifies as a low-mass galaxy.

4. Evidence for a Central Black Hole

4.1. X-Ray Detection

Combining observations from three separate epochs, with the first dominating the signal, HSC-XD 52 is strongly detected in the XMM soft (SB; $0.5 - 2$ keV), hard (HB; $2 - 10$ keV) and full (FB; $0.5 - 10$ keV) bands, with ≈ 109, 133, and 245 photon counts (in the PN+MOS1+MOS2 detectors), respectively (Chen et al. 2018). It has an FB luminosity of $L_X \approx 3.5 \times 10^{43}$ erg s^{-1} and an S/N of 185 (143) in the PN (M1) detector (see Table 1). The derived hardness ratio of

$$\mathrm{HR} \equiv \frac{H - S}{H + S} = 0.17 \pm 0.07, \qquad (1)$$

where H (S) is the total (all three detectors) net counts divided by the total exposure time in the HB (SB), is consistent with a Type I AGN at the redshift of HSC-XD 52. This XMM source is spatially coincident with the HSC optical source. Figure 1 provides the XMM image with the X-ray and HSC centroids marked as a black cross and a red circle ($1\rlap{.}''3$), respectively.

X-ray emission produced by stellar processes, such as that from X-ray binaries (XRBs), could mimic the accretion signatures of AGN. From Lehmer et al. (2010), the relation between XRB L_X, $M_\star$, and SFR is

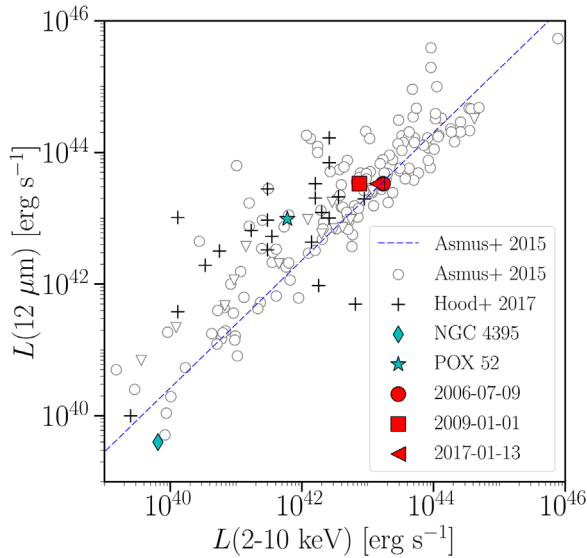$$L_{X,\mathrm{XRB}} = (\alpha M_\star + \beta \mathrm{SFR}) \text{ erg s}^{-1}, \qquad (2)$$

Figure 3. Observed correlation between IR luminosity at $\lambda = 12\ \mu$m and X-ray luminosity at 2–10 keV with the best-fit from Asmus et al. (2015; dashed blue line). $L(12\ \mu$m) is not measured directly but extrapolated using a power-law fit to the IRAC and MIPS data. We include data compiled from Asmus et al. (2015; all types of AGN; gray open symbols) and Hood et al. (2017; low-mass AGN; black crosses). Triangles indicate upper limits. Cyan symbols represent low-redshift analogs to HSC-XD 52, which is shown at early, intermediate, and late epochs as a red circle, square, and triangle (upper limit on X-ray luminosity), respectively.

with $\alpha = (9.05 \pm 0.37) \times 10^{28}\ M_\odot^{-1}$ and $\beta = (1.62 \pm 0.22) \times 10^{39}\ (M_\odot\ \mathrm{yr}^{-1})^{-1}$. We have focused on high-mass XRBs because these dominate at $L_X \gtrsim 10^{39}\ \mathrm{erg\ s}^{-1}$ (Lehmer et al. 2010). Our best estimates of $M_\star$ and SFR (Table 1) generate an expected luminosity due to XRBs of $L_{X,\mathrm{XRB}} \approx 9.6 \times 10^{39}\ \mathrm{erg\ s}^{-1}$, several orders of magnitude lower than that observed. Even adopting conservative upper limit values for SFR and $M_\star$ results in $L_{X,\mathrm{XRB}} \ll 10^{43}\ \mathrm{erg\ s}^{-1}$.

HSC-XD 52 was observed with XMM three separate times spanning over a decade: first on 2006 July 9, next on 2001 January 1, and finally on 2017 January 13. The first two observations yielded fluxes (in cgs) of $(1.35 \pm 0.28) \times 10^{-14}$ and $(5.92 \pm 1.45) \times 10^{-15}$ from the PN detector alone. During the final epoch of observation, the source was detected only by the MOS2 detector because it fell on a dead chip of the MOS1 detector, and in a chip gap on the PN detector. Thus, this final observation yields only a weak upper limit on the flux (in cgs) of $< 1.10 \times 10^{-14}$. In Figure 3, we compare HSC-XD 52 at the three different epochs to other X-ray luminous AGN observed with high spatial resolution ground-based mid-IR imaging (Asmus et al. 2015) and low-mass AGN from Hood et al. (2017). HSC-XD 52 falls on the empirical correlation (within the uncertainties) measured by Asmus et al. (2015) at least for the first two epochs. We also find the properties of HSC-XD 52 at these epochs to be consistent with other observed correlations (e.g., L_X–[O III]), further bolstering our confidence in its characterization as an AGN. Comparing HSC-XD 52 with itself over the three epochs, it is clear that its X-ray luminosity is fading over time, suggesting a corresponding fall in activity.

To derive a lower limit on M_{BH}, we can assume HSC-XD 52 is radiating at the Eddington luminosity when activity is highest. We assume a bolometric luminosity as determined by the best-fit SED model of $L_{\mathrm{AGN}} = 1.20 \times 10^{44}\ \mathrm{erg\ s}^{-1}$, which is also consistent with applying a typical bolometric correction

to the observed L_X at this earliest epoch. This yields a lower limit of

$$M_{\mathrm{BH}} \gtrsim \left(\frac{L_{\mathrm{AGN}}}{1.26 \times 10^{38}\ \mathrm{erg\ s}^{-1}} \right) M_\odot$$
$$\gtrsim 9.5 \times 10^5 M_\odot. \tag{3}$$

4.2. Spectral Diagnostics

An SDSS spectrum from 2013 November 9 is publicly available for this source. In addition, we acquired a spectrum with MagE on 2019 July 27. The SDSS spectrum is dominated by strong [O III] and Balmer emission lines. Our modeling of these lines, especially Hα and Hβ, favors a broad-line component, suggesting the presence of an AGN contributing to the observed flux. However, the more recently acquired MagE spectrum, which has better resolution and higher S/N, does not exhibit broad lines. In Figure 4, we show zoom-ins of the [O III 4959, 5007] doublet from the MagE spectrum (bottom panel) and the Hα lines (top panel) from both the SDSS (left) and MagE (right) spectra. In red, we show our best-fit models for these lines, with dashed lines representing single-component Gaussians and solid lines representing composite Gaussians consisting of both broad and narrow components. While the SDSS spectrum favors some broad components in the Hα line, the MagE Hα line is consistent with the [O III] doublet. We note that the Hβ emission in the MagE is blended with a strong sky line in the MagE spectrum, making it unreliable for an accurate line profile measurement.

Using the SDSS spectrum, for which we find broad Hα and Hβ alone, we measure an FWHM of $\mathrm{FWHM}_{\mathrm{H}\alpha} = \mathrm{FWHM}_{\mathrm{H}\beta} \approx 1076\ \mathrm{km\ s}^{-1}$. From this spectrum, we also measure the continuum luminosity at $\lambda = 5100$ Å of $L_{5100} \approx 1.8 \times 10^{43}\ \mathrm{erg\ s}^{-1}$. Our SED modeling suggests that at this wavelength in the continuum, the AGN emission dominates compared to the starlight by a factor of ≈ 5 (bottom panel of Figure 2). We can then apply the virial formula presented as Equation (5) of Greene & Ho (2005) to estimate an effective upper limit on the black hole mass of $M_{\mathrm{BH}} \lesssim 1.7 \times 10^6 M_\odot$. While this mass estimate is consistent with that based on the Eddington argument, we emphasize that it is based on a somewhat equivocal broad-line detection.

As an additional verification of HSC-XD 52's AGN nature, we also measured the [O I 6300] emission line. The ratios of [O I 6300]/Hα and [O III 5007]/Hβ allow us to place the source on an emission line diagnostic diagram, where it falls securely within the Seyfert region (e.g., Kewley et al. 2006) during the epoch of the SDSS spectrum.

5. Discussion and Conclusion

We have presented photometric and spectroscopic observations of HSC-XD 52, an object identified as part of a new search for X-ray selected low-mass AGN in the HSC survey. Our analysis suggests that HSC-XD 52 has a stellar mass of $M_\star \approx (3.0 \pm 0.7) \times 10^9 M_\odot$ and hosts a luminous accreting black hole with $M_{\mathrm{BH}} \approx 10^6 M_\odot$ and $L_X \approx 3.5 \times 10^{43}\ \mathrm{erg\ s}^{-1}$, though its X-ray luminosity (and thus accretion rate) is variable and appears to be decreasing with time. Its properties resemble those of known low-mass AGN hosts in the local universe, including POX 52 and NGC 4395. The detection of HSC-XD 52 provides convincing evidence for the existence of luminous
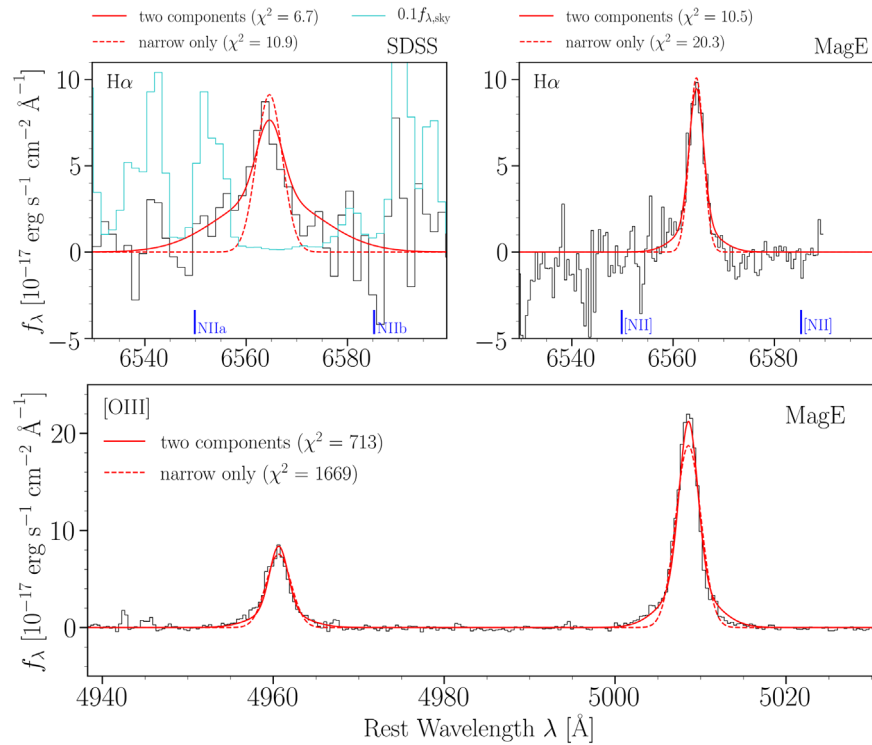
Figure 4. Zoom-ins of the SDSS (top left) and MagE (top right and bottom) spectra (black lines) with fitted models of important emission lines Hα (top panels) and the [O III 4959, 5007] doublet (bottom). We model each line (pair of lines, in the case of [O III]) as a two-component Gaussian (solid red line) or as single narrow component Gaussian (dashed red line). In the Hα zoom-ins (top), we also label where [N II] lines would fall if they were present. For the SDSS spectrum (top left), we overplot the sky spectrum scaled down by a factor of 10 (cyan line). None of these lines is highly contaminated, while Hα in particular falls conveniently between sky lines.

active MBHs in low-mass galaxies at this higher redshift. Further observations, particularly temporal monitoring in rest-frame optical, could reveal continuum variability and thus shed more light on the evolution of AGN activity.

By requiring an unambiguous XMM detection, our methodology selects for the most luminous sources at intermediate redshifts. This is clear when we compare HSC-XD 52 to other, more local low-mass AGN including POX 52 and NGC 4395. As a direct consequence of our search method and the source's higher redshift ($z \approx 0.56$), HSC-XD 52 lies on the brighter end of observed correlations (e.g., between mid-IR and X-ray luminosities; Figure 3). Outside of the very local universe, it is only for sources like this one that we can obtain a robust determination of the galaxy's low stellar mass, a confirmation of its AGN nature, and a well-constrained black hole mass.

The best-fit model to the observed correlation between $M_\star$ and M_{BH} for local broad-line AGN of Reines & Volonteri (2015) predicts $M_{BH} \approx 7.1 \times 10^5 M_\odot$ for HSC-XD 52, which is consistent with our estimate of the BH mass given the 0.55 dex scatter. With a larger sample of similar objects, we can begin to explore the relationship between M_{BH} and $M_\star$ for low-mass galaxies at intermediate redshifts in earnest.

To place meaningful constraints on statistical properties such as the occupation fraction as a function of redshift, we require a large sample with well-understood selection effects and biases, but significant challenges remain. While spectroscopic redshifts are cleaner, they impose a selection function on the samples used in past studies. Photometric redshifts are more inclusive, but often include undesirable contaminants as a repercussion, among other drawbacks (see details in G. Halevi et al. 2019, in preparation). Furthermore, probing the regime of lower-

luminosity X-ray sources requires unambiguously discriminating between stellar processes (i.e., XRBs) and accretion onto an MBH as the origin of the X-rays. This becomes increasingly difficult at $L_X \lesssim 10^{40}$ erg s^{-1}, which presents a significant obstacle to developing a clean sample of low-mass AGN that is representative of the underlying population while still covering a sufficiently large volume.

In the 2030s, the launch of the next-generation X-ray observatory Lynx (The Lynx Team 2018) would enable high-S/N X-ray spectra of AGN in dwarf galaxies, and with its high spatial resolution, localization of the X-ray emission, thus breaking the degeneracy between emission from AGN and stellar processes. Additionally, its sensitivity will facilitate X-ray detections of SMBH seeds at cosmological distances. Meanwhile, the space-based gravitational-wave detector LISA (Amaro-Seoane et al. 2017) will open the door to multi-messenger studies of early SMBHs. These future missions imply a promising future for the quest to illuminate the mysteries of how MBHs form and grow, and in turn, how their host galaxies evolve.

ORCID iDs

Goni Halevi ⓘ https://orcid.org/0000-0002-7232-101X
Sean D. Johnson ⓘ https://orcid.org/0000-0001-9487-8583
Hyewon Suh ⓘ https://orcid.org/0000-0002-2536-1633
Yoshiki Toba ⓘ https://orcid.org/0000-0002-3531-7863

References

Aihara, H., Arimoto, N., Armstrong, R., et al. 2018a, PASJ, 70, S4
Aihara, H., Armstrong, R., Bickerton, S., et al. 2018b, PASJ, 70, S8
Amaro-Seoane, P., Audley, H., Babak, S., et al. 2017, arXiv:1702.00786
Araya Salvo, C., Mathur, S., Ghosh, H., Fiore, F., & Ferrarese, L. 2012, ApJ, 757, 179
Asmus, D., Gandhi, P., Hönig, S. F., Smette, A., & Duschl, W. J. 2015, MNRAS, 454, 766
Astropy Collaboration, Price-Whelan, A. M., Sipőcz, B. M., et al. 2018, AJ, 156, 123
Astropy Collaboration, Robitaille, T. P., Tollerud, E. J., et al. 2013, A&A, 558, A33
Barth, A. J., Ho, L. C., Rutledge, R. E., & Sargent, W. L. W. 2004, ApJ, 607, 90
Bellovary, J., Volonteri, M., Governato, F., et al. 2011, ApJ, 742, 13
Bellovary, J. M., Cleary, C. E., Munshi, F., et al. 2019, MNRAS, 482, 2913
Bizzocchi, L., Filho, M. E., Leonardo, E., et al. 2014, ApJ, 782, 22
Blanton, M. R., Bershady, M. A., Abolfathi, B., et al. 2017, AJ, 154, 28
Boquien, M., Burgarella, D., Roehlly, Y., et al. 2019, A&A, 622, A103
Brandt, W. N., & Alexander, D. M. 2015, A&ARv, 23, 1
Bruzual, G., & Charlot, S. 2003, MNRAS, 344, 1000
Chabrier, G. 2003, PASP, 115, 763
Chen, C. T. J., Brandt, W. N., Luo, B., et al. 2018, MNRAS, 478, 2132
Dale, D. A., Helou, G., Magdis, G. E., et al. 2014, ApJ, 784, 83
Desroches, L.-B., & Ho, L. C. 2009, ApJ, 690, 267
Dong, X.-B., Ho, L. C., Yuan, W., et al. 2012, ApJ, 755, 167
Filippenko, A. V., & Ho, L. C. 2003, ApJL, 588, L13
Fritz, J., Franceschini, A., & Hatziminaoglou, E. 2006, MNRAS, 366, 767
Gliozzi, M., Satyapal, S., Eracleous, M., Titarchuk, L., & Cheung, C. C. 2009, ApJ, 700, 1759
Greene, J. E., & Ho, L. C. 2005, ApJ, 630, 122
Greene, J. E., & Ho, L. C. 2007, ApJ, 670, 92
Griffin, M. J., Abergel, A., Abreu, A., et al. 2010, A&A, 518, L3
Groves, B. A., Heckman, T. M., & Kauffmann, G. 2006, MNRAS, 371, 1559
Ho, L. C., Filippenko, A. V., & Sargent, W. L. W. 1997, ApJS, 112, 315
Hood, C. E., Barth, A. J., Ho, L. C., & Greene, J. E. 2017, ApJ, 838, 26
Jarvis, M. J., Bonfield, D. G., Bruce, V. A., et al. 2013, MNRAS, 428, 1281
Kewley, L. J., Groves, B., Kauffmann, G., & Heckman, T. 2006, MNRAS, 372, 961
Kormendy, J., & Ho, L. C. 2013, ARA&A, 51, 511
Lehmer, B. D., Alexander, D. M., Bauer, F. E., et al. 2010, ApJ, 724, 559
Lemons, S. M., Reines, A. E., Plotkin, R. M., Gallo, E., & Greene, J. E. 2015, ApJ, 805, 12
McAlpine, W., Satyapal, S., Gliozzi, M., et al. 2011, ApJ, 728, 25
Mezcua, M., Civano, F., Marchesi, S., et al. 2018, MNRAS, 478, 2576
Miller, B. P., Gallo, E., Greene, J. E., et al. 2015, ApJ, 799, 98
Moran, E. C., Shahinyan, K., Sugarman, H. R., Vélez, D. O., & Eracleous, M. 2014, AJ, 148, 136
Moutard, T., Arnouts, S., Ilbert, O., et al. 2016, A&A, 590, A103
Nguyen, D. D., Seth, A. C., Neumayer, N., et al. 2019, ApJ, 872, 104
Noll, S., Burgarella, D., Giovannoli, E., et al. 2009, A&A, 507, 1793
Pardo, K., Goulding, A. D., Greene, J. E., et al. 2016, ApJ, 831, 203
Reines, A. E., Greene, J. E., & Geha, M. 2013, ApJ, 775, 116
Reines, A. E., Plotkin, R. M., Russell, T. D., et al. 2014, ApJL, 787, L30
Reines, A. E., & Volonteri, M. 2015, ApJ, 813, 82
Satyapal, S., Böker, T., Mcalpine, W., et al. 2009, ApJ, 704, 439
Sawicki, M., Arnouts, S., Huang, J., et al. 2019, MNRAS, 489, 5202
Schramm, M., Silverman, J. D., Greene, J. E., et al. 2013, ApJ, 773, 150
Secrest, N. J., Satyapal, S., Gliozzi, M., et al. 2012, ApJ, 753, 38
She, R., Ho, L. C., & Feng, H. 2017, ApJ, 842, 131
The Lynx Team 2018, arXiv:1809.09642